JOURNAL OF MATERIALS SCIENCE **34** (1999) 3801–3812

Solid state sintering of ceramics: pore microstructure models, densification equations and applications

J. L. SHI
State Key Lab. of High Performance and Superfine Microstructure, Shanghai Institute of Ceramics, Chinese Academy of Sciences, 1295 Ding-Xi Road, Shanghai, 200050, People's Republic of China

The stability of closed pores in two and three dimensions has been discussed and it is found that the stability of pores in two dimension can be determined mathematically from their particle coordination number and dihedral angle; while those in three dimension can be approximately determined by a spherical pore model. This model is set up by first excluding the effect of interface tension, so the pore was supposed to be spherical, and then the tensile stress arising from the interface tension was allowed to act on this hypothesized spherical pore. On the basis of the spherical pore model, pore microstructure models for real powder compacts were set up and the densification equations for the intermediate and final stages of sintering were derived. The criterion for pore shrinkage, and the effect of pore size distribution and green density were discussed according to the derived equations. The densification equations for pressureless solid state sintering can be easily extended to describe the densification behaviour during hot-pressing or hot-isostatic-pressing. Densification characteristics in liquid state sintering were also considered from the result of solid state sintering.

1. Introduction

1.1. Sintering stages and existing solid state sintering models and theories

1.1.1. About sintering stages

For advanced ceramics, densification is the essential process for sintering, and full densification is a prerequisite for the achievement of their intrinsic properties. Densification in pressureless sintering is related to the system itself, and densification theory in pressureless sintering has been a fundamental theme for several decades [1–11]. Pressureless sintering can either be liquid state sintering or solid state sintering where only solid phase(s) is present in the system during densification. The present paper is mainly concerned with solid state sintering.

According to Coble [12, 13], solid state sintering can be divided into three stages. The first or initial stage of sintering involves interface formation and neck growth between primary particles (the contact area between the particles increases from zero (ideally point contact)) to a certain extent, and the neck growth will cease when an equilibrium configuration is reached. The initial stage of sintering, as indicated by Coble, involves no grain growth.

The second or intermediate stage of sintering starts when grain growth begins. During this stage of sintering, grain boundaries form extensively but pores are still connected with each other and form a continuous pore network, i.e., pore channels exists, while the grain boundaries are still isolated and no continuous grain boundary networks are formed. Most densification and microstructure changes take place in this stage of sintering.

As pores become isolated and grain boundaries form a continuous network, the intermediate stage of sintering ends and the third or final stage of sintering starts. In the final stage of sintering, isolated pores are located at grain boundaries (interfaces), or linear junctures of three grains or point junctures of four grains, and/or entrapped in grains. Density increases slightly but the microstructure develops (grains grow) very rapidly in this stage of sintering.

1.1.2. Models for the initial stage of sintering

Based on a similar two-sphere model numerous densification equations were developed by different authors [14–20] to describe the densification processes in the initial stage of pressureless sintering. The densification equations were derived by supposing that the linear shrinkage rate of a sintered compact is equal to the rate of approach of the centers of two spheres. In this way, material transport by surface diffusion, vapor-condensation, or volume diffusion from surface to the neck area were assumed to have no contributions to the densification, while those by viscous flow, grain boundary diffusion and the volume diffusion from boundary

to the neck area were considered to contribute. The total shrinkage in this stage of sintering is very limited [18, 19]. A detailed summary of the sintering theories in the initial stage of sintering can be found in the Exner's review paper [18].

1.1.3. Model for the intermediate stage of sintering

The sintering phenomena in this stage of sintering are much more complicated because of the complexity of the densification process itself and the interference from grain and pore growth on densification, which leads to difficulties in setting up an appropriate model describing the process. In the early 60s, Coble [12, 13] put forward a microstructure model for materials transport (diffusion)—a tetrakaidecahedron with cylindrical pores located at each edge. With this model, a densification equation was derived and the relation between the porosity remaining in the sintered body and the sintering time was obtained. This model has been accepted as the derived porosity-time relation fitted well with the experimentally observed linear relationship between density and the logarithm of time.

After Coble's model, only limited progress has been made on modeling the intermediate stage of sintering on a similar microstructure scale. Johnson [21] after Coble reported a similar revised model but with no major variations.

Coble's model is oversimplified, as has been found by many researchers [18, 19]. In addition, the model can not be used to explain several important sintering phenomena. The effect of agglomerates on densification, for example, as has been pointed out in the last two decades, is very significant for fine powders, and Coble's theory was unable to explain this. This is, most probably, because the effect of interface tension, and thus the thermodynamic stability of pores, was not considered in his model. Experimentally, the linear relation between densities and the logarithm of time obtained by Coble under the assumption of a cubic grain growth law is also true for sintering process such as hot-pressing where very limited grain growth was observed [22–24], and furthermore, phenomenological fitness with the relation does not necessarily convey physical meanings [18, 19, 25]. As has been found by Pejovnik and coworkers [26], the process can be fitted to other forms of simple empirical equations [26, 27], if appropriate parameters were selected for the equations. A detailed analysis about Coble's model and his derivation of the densification equations will be given in Section 5.

1.1.4. Theories for the final stage of sintering

Similar to the intermediate stage, there are no satisfactory theories describing the densification process in this stage of sintering. By making use of and slightly modifying his microstructural model for sintering in the intermediate stage, Coble gave a similar relation between porosity and time [12], which is far less satisfactory than for the intermediate stage because of the non-existence of a linear relation between porosity and the logarithm of time in this stage of sintering.

A significant progress for characterizing the final stage microstructure development has been made by Harmer *et al*. [28, 29]. A microstructure map was developed which mainly involves the relation between the grain size and pore size, or more importantly, the relation between the grain size and the relative density. However, a direct densification equation was not available.

1.1.5. Other theories for the solid stage of sintering

In addition to the traditional microstructure (diffusion) model for solid state sintering, there are some other macro- or statistical sintering models being developed [30–32]. In the present author's opinion, however, these models are of limited significance as they involve some self-defined parameters which have no definite physical meaning, and a densification equation for solid state sintering is not available in these theories.

1.1.6. Contributions of the different sintering stages to densification

It is obvious that most of theories are for the first stage of sintering based mostly on a two identical sphere model [18, 19]. The densification contribution in the early stage of sintering is very limited, and far from accounting for all the sintering process. Many experiments for the sintering of very large metal sphere showed that the linear shrinkage was less than 10% [18, 19], and in fact regularly at around 2–3%. For real ceramic powder compacts, grain growth (i.e., coarsening) will occur during heating so the densification contribution in this stage is further decreased. The final stage of sintering generally starts at the relative densities of $\geq$90% and so the most densification takes place in the intermediate stage of sintering, and therefore, more attention should be paid to this stage of sintering. Unfortunately, the model description and theoretical analysis for the intermediate stage of sintering is much less than those for the early stage of sintering.

1.2. The interaction between surface tension and interfacial tension

1.2.1. The driving force for the densification

The densification process of a powder compact is accompanied by a decrease of the surface area and the formation of interfaces, i.e., the surface tension is the driving force for densification and the interface is the resistance to densification. The whole driving force is:

$$\Delta G = \Delta G_s + \Delta G_i = \gamma_s \, dA_s + \gamma_i \, dA_i \qquad (1)$$

where ΔG, ΔG_s and ΔG_i are the changes of the total free energy, surface energy and the interface energy; γ_s and γ_i are the surface and interface tension and A_s and A_i are the specific surface and interfacial areas.

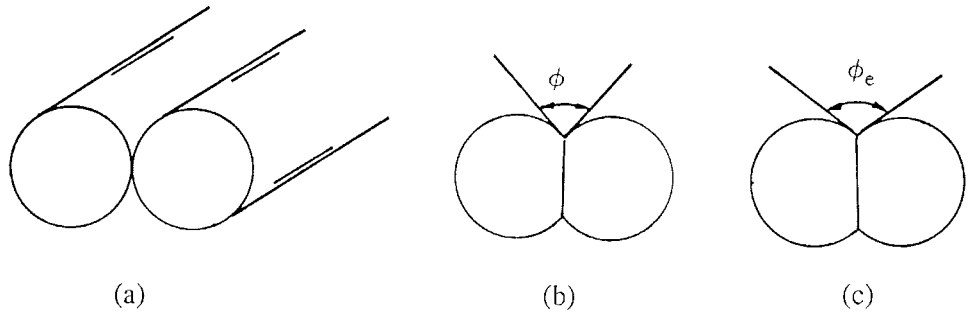

Figure 1 Schematics of the formation of dihedral angle between two identical touching cylinders, (a) particles in touch, (b) neck formation, $0 < \phi < \phi_e$, (c) equilibrium configuration, $\phi = \phi_e$.

1.2.2. Chemical potential for the neck formation and mass transport

Considering the two sphere model, neck formation between two particles is driven by the differential chemical potential between the neck area and the particle surface. When the formation of interface area is not considered at first, the chemical potential, $\Delta\mu_n$, or, the driving force for the neck formation, according to the Gibbs-Kelvin relation, will be:

$$\Delta\mu_n = \gamma_s\Omega(1/\rho_n - 1/r) \quad (2)$$

where Ω is the atomic volume, ρ_n and r are the radii of the neck and the particles. As the neck surface is concave judged from particles (circle center of neck is out of particle), $\rho_n < 0$.

In addition to the neck formation process between particles, there is the chemical potential for mass transport within a particle or between particles, and this chemical potential, defined as $\Delta\mu_c$, is:

$$\Delta\mu_c = \gamma_s\Omega[(1/r_{1i} + 1/r_{1ii}) - (1/r_{2i} + 1/r_{2ii})] \quad (3)$$

where r_{1i}, r_{1ii} and r_{2i}, r_{2ii} are the orthogonal principal radii within one particle at place '1' and place '2', or the orthogonal principal radii of two different particles ($r_1 > r_2$) for particle '1' and particle '2'. To simplify the equation, let $2/r_1 = 1/r_{1i} + 1/r_{1ii}$, and $2/r_2 = 1/r_{2i} + 1/r_{2ii}$, Equation 3 becomes:

$$\Delta\mu_c = 2\gamma_s\Omega(1/r_1 - 1/r_2) \quad (3')$$

It can be seen from Equation 3, if there is a difference of the radius of curvature (the particle is not a sphere), mass transport would take place from the area of larger curvature (smaller curvature radii) to the area of smaller curvature (larger curvature area) till the particle becomes a sphere (where $r_{1i} = r_{1ii} = r_{2i} = r_{2ii}$); and if two spheres of different radius (where r_1 and r_2 are the radii of them) are in contact, there will be the mass transport between them from the smaller one to larger one till the two particles become one sphere. This process has been generally related to particle coarsening.

Neck formation between two spheres is accompanied by a change of the particle shape. Some authors believed [20] that neck formation can be accomplished only with mass transport from adjacent to the neck, and therefore form a *so-called* undercutting configuration close to the neck. However, this will probably not happen, as the formation of undercutting, thermodynamically according to Equations 3 and 3′, increases the free energy of the system and the spherical particles would keep their spherical shape during neck formation.

1.2.3. Dihedral angle and the coordination number

Considering a simple example of two touching cylinders of the same diameter with infinite length (Fig. 1). The neck will grow during sintering, and the contact angle (ϕ) between the two adjacent surfaces of the two cylinders increases from zero till a constant value of ϕ_e where the system reaches an equilibrium configuration, and ϕ_e is the *so-called* dihedral angle:

$$\cos\phi_e/2 = \gamma_i/2\gamma_s \quad (4)$$

This relation, though simple, is basic in explaining the thermodynamics of pores in sintering [12, 13].

As a pore is coordinated by particles, it is therefore surrounded by pore-particle surfaces and particle-particle interfaces, so pore stability must be affected by the particle coordination number. This concept was first put forward by Kingery and Francois [33] and later developed by Lange [34] and Shi [35]. A critical particle coordination number for the stability of a pore can be given as discussed in the following sections of this paper.

1.3. The relation between the grain growth and the densification

Traditionally grain growth (or coarsening) during sintering is regarded as an interference or impedance to densification. By studying the relation between densification and grain size of some particle arrays, Lange [36, 37] suggested that grain growth via coarsening can continually drive sintering by reinitiating sintering when a metastable equilibrium configuration (or dihedral angle) for the particle array is reached. By this means, Lange *et al.* [34] gave an explanation for the linear relation between densities and grain size for sintered alumina, which was found by Gupta [38] two decades ago. The relation between densification and grain growth will be discussed in the second paper of this series [39].

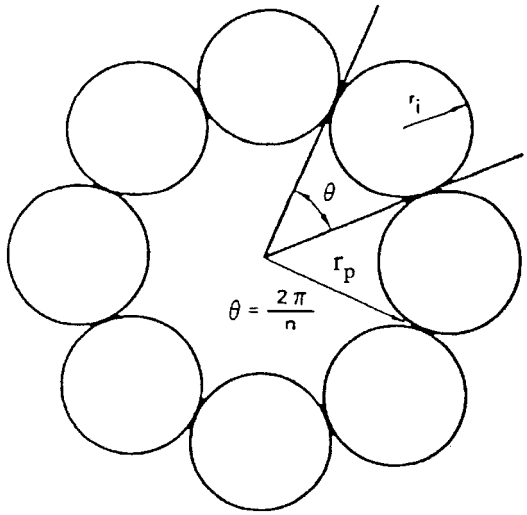

Figure 2 A two dimensional pore surrounded by n cylinders.

2. Pore stability—a spherical pore model

2.1. Stability of a two dimensional pore determined by mathematical analysis

The stability of a pore in two dimension was discussed by Kingery *et al.* [33], and Lange [34] further put forward the concept of the particle coordination number of pores in three dimensions. A quantitative mathematical analysis will be given as follows.

Fig. 2 shows a two dimensional pore surrounded by n cylinders. The dihedral angle can also be established between two touching surfaces, but the pore stability is determined by both the dihedral angle and the particle coordination number for the pore. Fig. 3 is the pore configuration under different particle coordination numbers. Let ρ_r, r_p and n be the curvature radius of the pore particle surface, the radius of its circumscribed circle and the coordination number respectively (see Fig. 4), from Fig. 4 we have:

$$\rho_r \times \sin\alpha = \sin\beta \times r_p \tag{5}$$

as

$$\beta = \pi/n \tag{6}$$

and

$$\alpha = \pi/2 - \phi = \pi/2 - (\pi/2 - \pi/n + \pi/2 - \phi/2) = \phi/2 - \pi/2 + \pi/n \tag{7}$$

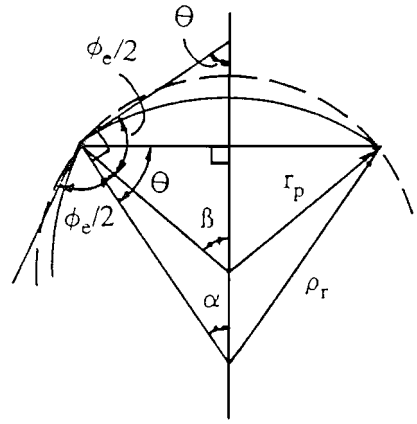

Figure 4 Schematics for the relation between ρ_r and r_p (for details see text).

so the relations among these parameters can be determined:

$$\rho_r = \frac{\sin(\pi/n)}{\sin\left(\frac{\phi_e}{2} - \frac{\pi}{2} + \frac{\pi}{n}\right)} \cdot r_p \tag{8}$$

where ϕ_e is the dihedral angle and n is the coordination number for the pore. As the radius of the circumscribed circle changes, the free energy of the systems will change, as can be described as

$$dG = n\gamma_s \cdot 2\alpha\, d\rho_r - n\gamma_i\, dr_p \tag{9}$$

where 2α is the radian faced by every pore-particle surface. Dividing Equation 9 by dr_p, and combining Equations 7 and 8 into the above equation:

$$\frac{dG}{dr_p} = \frac{\phi_e - \pi + \frac{2\pi}{n}}{\sin\frac{1}{2}\left(\phi_e - \pi + \frac{2\pi}{n}\right)} \cdot \sin\frac{\pi}{n} n\gamma_s - n\gamma_i \tag{10}$$

So, we have the following criterion for the pore stability for $dG/dr_p = 0$:

$$n_c = 2\pi/(\pi - \phi_e) \tag{11}$$

If $n = 2\pi/(\pi - \phi_e) = n_c$, $\rho_r = \infty$, and the particle surface is a plane, the system is at equilibrium, n_c is the critical coordination number for a two-dimensional pore in a plane; if $n < n_c$, $\rho_r > 0$, the particle surface is convex

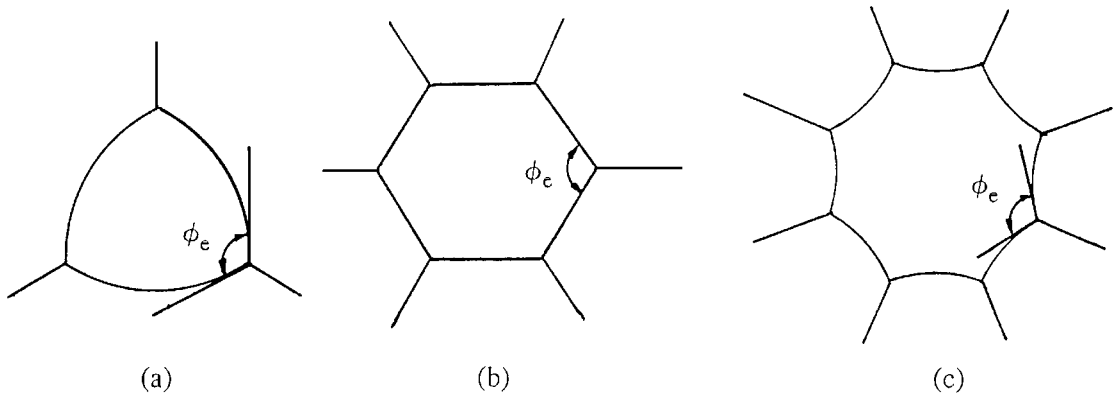

Figure 3 Schematics of the two dimensional pore configurations, (a) $\rho_r > 0$, $n < n_c$; (b) $\rho_r = 0$, $n = n_c$ and (c) $\rho_r < 0$, $n > n_c$.

judged from the pore center, $dG/dr_p > 0$, the free energy of the system will increase as the pore grows (its radius r_p increase); if $n > n_c$, $\rho_r < 0$, the particle surface is concave judged from the pore centers, and $dG/dr_p < 0$, the free energy of the system will decrease as the pore grow. The pore configurations of different values of ρ_r at a given dihedral angle are schematically illustrated in Fig. 3.

2.2. Stability of a three-dimensional pore (the pore in space)

The stability problem of a three-dimensional pore (a pore in space) is much more difficult to deal with because the pore in practice is not a sphere. To simplify the problem, the curvature of the pore-particle surface led by the dihedral angle and the coordination number is first to be ignored temporarily, i.e., at first the effect of interface energy is not considered, so under this hypothesis this could be assumed that $\phi_e = \pi$, i.e., the pore was a 'sphere' and the pore-particle surface energy would be $4\pi r^2\gamma_s$, thus the driving stress for the pore shrinkage σ_s is:

$$\sigma_s = \frac{d(4\pi r^2\gamma_s)}{dr} \cdot \frac{1}{4\pi r^2} = \frac{2\gamma_s}{r} \tag{12}$$

On this basis, supposing that the stress, σ_i for the pore expansion resulted from the interface energy acts on this hypothesized 'sphere', will approximately be:

$$\sigma_i = \frac{d(n \cdot l \cdot 2\gamma_i \cdot r)}{dr} \cdot \frac{1}{4\pi r^2} = \frac{n_s}{2\pi} \cdot \frac{l\gamma_i}{r^2} \tag{13}$$

where n_s is the coordination number of grains surrounding the pore in space (three-dimensional coordination number), l is the grain boundary length between two particles which face to the pore center (here the pore-particle surface is a part of the 'sphere' surface and the boundaries are arcs on the sphere surface with the same edge length).

The two stresses are both perpendicular to the pore sphere's surface but have opposite directions, so the compressive stress, σ_p, acting on the pore will be:

$$\sigma_p = \sigma_s - \sigma_i = \frac{2\gamma_s}{r} - \frac{n_s l\gamma_i}{2\pi r^2} \tag{14}$$

The stability of pores in three dimensions now can be explained on the basis of the spherical model and Equation 14 for the three-dimensional pores (closed pores).

3. Microstructure models for pores in sintering

3.1. The models and the deviation analysis

The above supposed spherical pore is fully surrounded by grains without pore openings. In the intermediate stage of sintering, the pores are connected with each other through these openings and form a continuous open network. With the help of the above pore model, the pores in the intermediate stage of sintering are still assumed to be spherical but with several openings

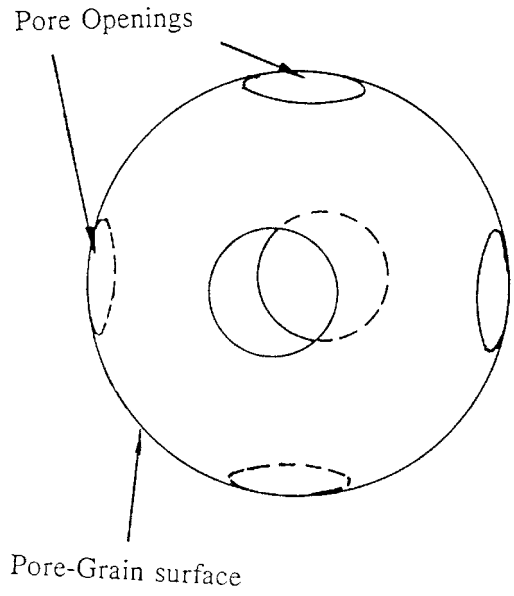

Figure 5 Schematics of the spherical pore microstructure model in space with six openings on the pore surface (for the intermediate stage of sintering).

which connect to other pores, as shown in Fig. 5 as a schematic drawing of the model with six openings. Without the openings, the model put forward for the intermediate stage of sintering can be directly applied to the final stage of sintering.

Deviations form the model are mainly in the calculation of the surface energy as the real surface area is certainly different from the spherical surface area. The magnitude of the deviation depends on the shape of the real pores. For the special case of a cubic pore (particle coordination number of 6 and dihedral angle of 90°), the surface area calculated from the cube is 18.8% smaller than the circumscribed sphere, but for a higher or a slightly smaller dihedral angle at fixed coordination number, and a different coordination number than 6, the deviations will be less than this value.

3.2. The space coordination number of a pore

The coordination number in three dimensions (in space) can be related to the size ratio between the pore and its surrounding particles. Let d and D be the volume equivalent diameters (diameter of a sphere of the same volume as the concerned particle or pore) for a pore and particles, and define R as the size ratio of pores to particles. If pores and particles are monosized and have the diameters d and D, respectively, we have:

$$R = d/D \tag{15}$$

and when there is a limited size distribution of pores and particles, the average sizes of which are $\bar{d}$ and $\bar{D}$, the ratio $\bar{R}$ is defined as:

$$\bar{R} = \frac{\bar{d}}{\bar{D}} \tag{16}$$

R or $\bar{R}$ here represent the state of densification, the decrease of $\bar{R}$ means pore shrinkage and densification

and the increase of $\bar{R}$, in contrast, represents a decrease of density.

Let n_s be the particle coordination number of a pore in space, the inter-particle edge length facing the pore be l, the inter-pore-particle area density be ρ' (ρ' will be less than one in the intermediate stage but be one in the final stage of sintering), then through the calculation of the surface area, we have:

$$n_s l^2/\rho' = \pi d^2$$

or

$$n_s = \pi \rho' d^2/l^2 \tag{17}$$

For the final stage of sintering, setting $\rho' = 1$, we have:

$$n_s = \pi d^2/l^2 \tag{18}$$

3.3. The compressive stress on the pore

For a 'spherical' pore fully surrounded by grains, the compressive stress has been derived as can be seen in Equation 14, but for a spherical pore with openings in it, the compressive stress will be a little different:

$$\sigma_p = \rho'\sigma_s - \sigma_i = \rho'\frac{2\gamma_s}{r_p} - \frac{n_s l \gamma_i}{2\pi r_p^2} \tag{19}$$

where σ_p, σ_s and σ_i are the total compressive stress, the compressive stress resulting from surface tension and the tensile stress resulting from interface tension on the pore, respectively and r_p is the radius of the pore. The decrease of the surface tension-related-compressive stress is reflected by the decreased pore-grain surface density, while that of the interface-related-tensile stress is reflected by the decreased coordination number and/or the grain edge length.

To get a concise relation between σ_p and R, the relation between l and d must be defined. Defining the particle shape surrounding a pore of radius $r_p = d/2$ as shown in Fig. 6 (treating the problem in two dimension), and assuming that the particle is a part of a sector with its radial size of $[(D+d)/2 - d/2]$, and the circumferential size is D at the radius of $(d+D)/2$, we have:

$$\begin{aligned} d/l &= (d+D)/l' = D(R+1)/l' \\ &= (R+1)[\sin(\pi/n)](\pi/n)^{-1} \end{aligned} \tag{20}$$

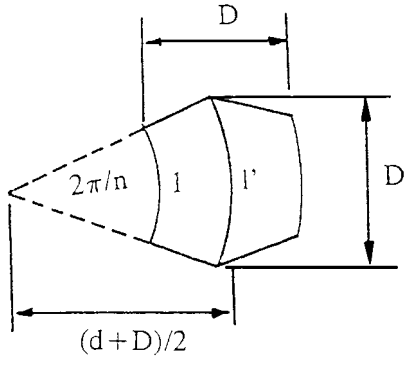

Figure 6 Schematics for the relation between d/l, R and n_s (for details see text).

where l and l' are the arc length at the radii of $d/2$ and $(d+D)/2$. From Equation 18, $n_s = n^2/\pi$:

$$\frac{d}{l} = (R+1)\frac{\sin(\pi/n_s)^{1/2}}{(\pi/n_s)^{1/2}} \tag{21}$$

Combining Equations 4, 17, 19 and 21 and the relation $d = 2r_p$, we obtain:

$$\sigma_p = \frac{4\gamma_s\rho'}{RD}\left[1 - (R+1)\frac{\sin(\pi/n_s)^{1/2}}{(\pi/n_s)^{1/2}}\cos\frac{\phi_e}{2}\right] \tag{22}$$

In the intermediate stage of sintering, the coordination number, n_s, is usually larger than 4 (e.g., in the close packing of spheres). To simplify the problem by assuming that at the intermediate stage of sintering, n_s is large enough for $\sin x = x$ then the above equation can be written as:

$$\sigma_p = \frac{4\gamma_s\rho'}{RD}\left[1 - (R+1)\cos\frac{\phi_e}{2}\right] \tag{23}$$

For the final stage of sintering, pores may be surrounded by less than 4 particles (e.g., $n_s = 1$ for pores within a grain, $n_s = 2$ for pores at boundaries), and $\rho' \to 1$, we have:

$$\sigma_p = \frac{4\gamma_s}{RD}\left[1 - (R+1)\frac{\sin(\pi/n_s)^{1/2}}{(\pi/n_s)^{1/2}}\cos\frac{\phi_e}{2}\right] \tag{24}$$

Equations 22–24 gives the sintering stresses for pores and are the basic relations which determine the stability of a pore thermodynamically.

4. Densification equations

4.1. Relation between densification rate and the pore volume shrinkage rate

Let ρ be the relative density of a sintering sample, V_T, V_S and V_P are the total volume, volume of solid phase and volume of pores in a unit weight, we have:

$$V_T = V_S + V_P, \quad V_T = 1/\rho, \quad V_P/V_T = 1 - \rho. \tag{25}$$

so,

$$\begin{aligned} \mathrm{d}\rho/\rho\mathrm{d}t &= -\mathrm{d}V_T/V_T\,\mathrm{d}t = -(V_P/V_T)\,\mathrm{d}V_P/V_P\,\mathrm{d}t \\ &= -(1-\rho)\,\mathrm{d}V_P/V_P\,\mathrm{d}t \end{aligned} \tag{26}$$

4.2. For a single pore

The volume change rate of a pore equals the diffusion flux of species (atoms or vacancies), and the flux is proportional to the effective diffusion coefficient and the driving force for the diffusion of the species, i.e., the chemical potential gradient, $\nabla\mu$. According to the diffusion equation by Herring [40] and later used by other researchers [41–43]:

$$|J| = (D_{eff}/\Omega_a kT)|\nabla\mu| \tag{27}$$

where $|J|$ is the absolute value of the species flux through unit area, D_{eff} is the effective diffusion

coefficient, Ω_a is the diffusion volume of the species and kT has the usual meaning.

The chemical potential gradient in the above equation can be approximately expressed as the chemical potential divided by the mean species diffusion distance, and this distance is assumed to be equal to the half of the sum of pore size and particle size, so:

$$|\nabla\mu| = 2\Delta\mu/(d+D) \tag{28}$$

The chemical potential $\Delta\mu$ equals the stress acted on the pore, σ_p, multiplied by the diffusion volume of the species:

$$\Delta\mu = \Omega_a\sigma_p \tag{29}$$

so when n_s is large enough for the intermediate stage:

$$|J| = \frac{4\gamma_s D_{eff}\rho'}{RDkt}\left[1-\cos\frac{\phi_e}{2}(R+1)\right]\frac{2}{d+D} \tag{30}$$

The relation of the pore volume change rate and $|J|$ is:

$$\frac{dV_p}{V_p\,dt} = -\frac{1}{\frac{1}{6}\pi d^3}\pi d^2\Omega_a|J| = -\frac{6\Omega_a}{d}|J| \tag{31}$$

approximately let $\rho' = \rho$, so the pore volume change rate can be expressed as:

$$\frac{dV_p}{V_p\,dt} = -\frac{48\Omega_a\rho\gamma_s D_{eff}}{D^3R^2(R+1)kT}\left[1-(R+1)\cos\frac{\phi_e}{2}\right] \tag{32}$$

Equation 32 is the densification equation for a single pore when $n_s \gg 1$.

When $dV_p/V_p\,dt = 0$, the pore is thermodynamically stable. There is then a critical R value, $R_c = (\cos\phi_e/2)^{-1} - 1$, which is the criterion for the pore stability. When $R < R_c$, the pores tend to shrink.

4.3. For compacts of mono-sized pores

Under a certain packing condition of particles, the size ratio, R, can be related to relative densities. For a compact with mono-sized pores and particles, defining K as the number of pores possessed by each particle (for a simple cubic packing $K = 1$), we have:

$$\rho = \frac{\frac{1}{6}\pi D^3}{\frac{1}{6}\pi D^3 + K\frac{1}{6}\pi d^3} = \frac{1}{1+KR^3} \tag{33}$$

so,

$$R = (K\rho)^{-1/3}(1-\rho)^{1/3} \tag{34}$$

Combining Equations 26, 32 and 34, the densification equation can be obtained:

$$\frac{d\rho}{\rho\,dt} = \frac{48K\rho^2(1-\rho)^{1/3}\Omega_a D_{eff}\gamma_s}{D^3\left[(K\rho)^{1/3}+(1-\rho)^{1/3}\right]kT} \times\left\{1-[(K\rho)^{-1/3}(1-\rho)^{1/3}+1]\cos\frac{\phi_e}{2}\right\} \tag{35}$$

The above formula is the densification rate equation for compacts with mono-sized pores. For such compacts, every pore shrinks, or, more accurately, the value of R decreases at the same rate, so the value of K is a constant in the intermediate stage of sintering and commonly K can be assumed to be 1. In addition, for a homogeneous compact with mono-sized pores, at higher packing densities and high dihedral angle:

$$1-[(K\rho)^{-1/3}(1-\rho)^{1/3}+1]\cos\frac{\phi_e}{2} \approx 1 \tag{36}$$

giving the condition:

$$\frac{d\rho}{\rho\,dt} = \frac{48\Omega_a\rho^2(1-\rho)^{1/3}D_{eff}\cdot\gamma_s}{D^3[\rho^{1/3}+(1-\rho)^{1/3}]kT} \tag{37}$$

4.4. For compacts with very narrow pore size distribution

For a real powder compact or sintering body, there will be pore size distributions. When the pore size distribution is narrow and an average value of the size ratio, R, can be used, substituting for the real R, so Equation 32 becomes:

$$\frac{d\rho}{\rho\,dt} = \frac{48\rho(1-\rho)\Omega_a D_{eff}\gamma_s}{D^3\bar{R}^2(\bar{R}+1)kT}\left[1-(\bar{R}+1)\cos\frac{\phi_e}{2}\right] \tag{38}$$

and the final densification equation under this condition will be approximately the same as Equation 35. For homogeneous compacts with high enough packing densities, $R < R_c$, all pores tend to shrink, and the compacts will densify. For $R > R_c$, e.g., loosely but homogeneously packed superfine powders, densification will be impossible.

4.5. For compacts of broad pore size distributions

For these powder compacts, where the value of R distributes equivalently broad like the pore size, the above equations can no longer be used. Pores of $R < R_c$ tend to shrink, but pores of $R > R_c$ are thermodynamically stable or tend to grow. Let $f(R)$ be the frequency distribution of R, there will be:

$$\bar{R} = \int_{R_{min}}^{R_{max}} Rf(R)\,dR \tag{39}$$

so the compressive stress on the sintering body will be:

$$\sigma_p = \frac{4\rho\gamma_s}{RD}\left[1-\int_{R_{min}}^{R_{max}}(R+1)f(R)\,dR\cos\frac{\phi_e}{2}\right] \tag{40}$$

and:

$$\frac{d\rho}{\rho\,dt} = \frac{48\Omega_a\rho(1-\rho)D_{eff}\cdot\gamma_s}{D^3\bar{R}^2(R+1)kT} \times\left[1-\int_{R_{min}}^{R_{max}}(R+1)f(R)dR\cos\frac{\phi_e}{2}\right] \tag{41}$$

The pores of $R > R_c$ are thermodynamically stable, and though these pores will theoretically tend to grow,

practically it was not evidently observed. So Equation 41 should probably be written as:

$$\frac{\mathrm{d}\rho}{\rho\,\mathrm{d}t} = \frac{48\Omega_a\rho(1-\rho)D_{\mathrm{eff}}\gamma_s}{D^3\bar{R}^2(\bar{R}+1)kT} \times\left[1-\int_{R_{\min}}^{R_c}(R+1)f(R)\cos\frac{\phi_e}{2}\,\mathrm{d}R\right] \cdot\int_{R_{\min}}^{R_c} f(R)\,\mathrm{d}R \quad (42)$$

The above formula is a general equation for powder compacts.

4.6. Densification equations in the final stage of sintering

With the help of the pore microstructure model for the final stage of sintering, and deriving the equation similar to those for the intermediate stage of sintering, following equations can be obtained:

$$\frac{\mathrm{d}V_p}{V_p\,\mathrm{d}t} = \frac{48\Omega_a D_{\mathrm{eff}}\gamma_s}{D^3R^2(R+1)kT} \times\left[1-(R+1)\frac{\sin(\pi/n_s)^{1/2}}{(\pi/n_s)^{1/2}}\cos\frac{\phi_e}{2}\right] \quad (43)$$

for a single pore with the critical R value being $R_c = (\cos\phi_e/2)^{-1}(\pi/\sqrt{n_s})(\sin\pi/\sqrt{n_s})^{-1}-1$; and

$$\frac{\mathrm{d}\rho}{\rho\,\mathrm{d}t} = \frac{48K\rho(1-\rho)^{1/3}\Omega_a D_{\mathrm{eff}}\cdot\gamma_s}{D^3\left[(K\rho)^{1/3}+(1-\rho)^{1/3}\right]kT} \cdot\left\{1-\left[1+(K\rho)^{-1/3}\cdot(1-\rho)^{1/3}\right] \times\frac{\sin(\pi/n_s)^{1/2}}{(\pi/n_s)^{1/2}}\cos\frac{\phi_s}{2}\right\} \quad (44)$$

or approximately let $\rho\approx 1$, and $1-\rho\approx 0$:

$$\frac{\mathrm{d}\rho}{\rho\,\mathrm{d}t} \approx \frac{48K^{2/3}(1-\rho)^{1/3}\Omega_a D_{\mathrm{eff}}\gamma_s}{D^3kT} \times\left[1-\frac{\sin(\pi/n_s)^{1/2}}{(\pi/n_s)^{1/2}}\cos\frac{\phi_e}{2}\right] \quad (45)$$

for mono-sized pores; and

$$\frac{\mathrm{d}\rho}{\rho\,\mathrm{d}t} \approx \frac{48\Omega_a(1-\rho)D_{\mathrm{eff}}\gamma_s}{D^3\bar{R}^2(\bar{R}+1)kT} \times\left[1-(\bar{R}+1)\frac{\sin(\pi/n_s)^{1/2}}{(\pi/n_s)^{1/2}}\cos\frac{\phi_e}{2}\right] \quad (46)$$

for sintering bodies of very narrow pore size distribution; and

$$\frac{\mathrm{d}\rho}{\rho\,\mathrm{d}t} = \frac{48(1-\rho)\Omega_a D_{\mathrm{eff}}\gamma_s}{D^3\bar{R}^2(\bar{R}+1)kT}\left[1-\int_{R_{\min}}^{R_c}(R+1)\,f(R) \times\frac{\sin(\pi/n_s)^{1/2}}{(\pi/n_s)^{1/2}}\cos\frac{\phi_e}{2}\mathrm{d}R\right]\cdot\int_{R_{\min}}^{R_c} f(R)\,\mathrm{d}R \quad (47)$$

for sintering bodies of broad pore size distribution. As for powder compacts with broad pore size distributions, the densification rate will be smaller than those of narrower pore size distribution. In the extreme case, the final stage of sintering may not be reached [35]. If it can be reached, the broad pore size distribution will, most probably, still exist [42–44].

5. Discussions

5.1. Pore shrinkage criteria

5.1.1. For pores in the intermediate stage of sintering

The essential criterion for a pore to shrink, under the condition $n_s \gg 1$, has been given in part 2.2, i.e., in the following simple equation:

$$R<R_c = (\cos\phi_e/2)^{-1}-1 \quad (48)$$

The equation is applicable for pores with large coordination numbers. When the coordination number n_s is not large enough, according to Equation 22:

$$R<R_c = \frac{(\pi/n_s)^{1/2}}{\sin(\pi/n_s)^{1/2}}\left(\cos\frac{\phi_e}{2}\right)^{-1}-1 \quad (49)$$

The criterion can be expressed with the coordination number, n_s. According to the relation between R and n_s (at high coordination number) from Equations 17, 20 and 48:

$$n_s^c = \pi\rho'(R_c+1)^2 = \pi\rho'\left(\cos\frac{\phi_e}{2}\right)^{-2} \quad (50)$$

It can be seen that for higher dihedral angle, the critical coordination number will be larger, and pores of $n_s<n_s^c$ can shrink, and the driving force for the pore shrinkage will be larger for larger critical coordination number.

5.1.2. For the final stage of sintering

Equation 49 can be used as the criterion of R value for the final stage of sintering. At an extreme condition, $n=1$, i.e., a pore within a grain, Equation 49 can be satisfied at any cases. The criterion of the coordination number(n_s), to simplify the problem, may approximate as:

$$n_s<n_s^c = \pi\left(\cos\frac{\phi_e}{2}\right)^{-2} \quad (51)$$

5.2. Sintering behavior of real powder compacts

5.2.1. Effect of pore size distributions

The densification of real powder compacts will be complicated as pore size is distributed in a certain range. If all the pores are thermodynamically unstable ($R<R_c$), all pores will tend to shrink, but smaller ones will shrink at higher rates than those of larger sizes (particles of different sizes are assumed to be homogeneously distributed). Stress [25] may therefore arise from the different densification rates between locations of different R values. The densification process of bodies with broader size distributions is usually slower than that

with narrower size distribution, as at the same compaction condition, compacts of broad size distribution usually contain a large amount of larger pores, probably caused by aggregates and/or agglomerates.

5.2.2. Effect of agglomerates

The existence of large agglomerates, e.g., hundred times larger than the primary particles would cause very broad pore size distributions in the powder compacts [34, 35, 45]. The primary pores among the primary particles are generally distributed in a limited range and easy to eliminate, while the secondary pores among agglomerates which are usually much larger and are of very large coordination number are difficult to remove. During densification and grain growth, the initially larger and thermodynamically stable pores are still difficult to remove because of the pore agglomerate effect led by grain growth, as has been reported by Francois and Kingery [46] in an investigation of the sintering behavior of UO_2. Studies by Zhao and Harmer [47] show that these very large but isolated pores in the final stage of sintering, though thermodynamically unstable and the pore agglomeration effect does not exist, are still difficult to remove by kinetic reasons.

Another aspect of the effect of agglomerates on sintering is reflected by the inter-action between agglomerates and un-agglomerated matrix when the agglomerate content is low, which leads to the crack-like defects in microstructures due to different shrinkage rates of agglomeraters and the matrix [45, 48].

5.2.3. Effect of green densities

Pores in bodies of higher green density will have smaller average R value and thus the densification is favored by (a) having a larger driving force for pore shrinkage and (b) having smaller diffusion distances. For sintering bodies of different densities but where all pores are thermodynamically unstable, the effect of green densities will be diminished with the progress of sintering, but for bodies of lower green densities, some pores with high R value will become thermodynamically stable, and densification will be greatly affected [44, 47].

5.2.4. Effect of entrapped gas on densification in the final stage of sintering

The effect of entrapped gas in pores in the final stage of sintering has been considered to impede densification by decreasing the effective dihedral angle [33]. For the present model, the gas pressure, P_g, can be directly incorporated into the sintering equation in the final stage of sintering:

$$\sigma_p = \frac{4\gamma_s}{RD}\left[1 - (R+1)\cos\frac{\phi_e}{2} - \frac{P_g D R}{4\gamma_s}\right] \qquad (52)$$

therefore the gas entrapped in pores will retard the densification process.

5.3. Comparison between the present densification equations and Coble's equations

As compared to the Coble's densification equations [12, 13], the present theory leads to consideration of the following additional, but important items:

(1) The effect of interface energy on densification was considered, and the concept of a pore stability criterion introduced, such that the effect of pore size distribution can be explained.

(2) The densification rate is related to the pore size: particle size ratio, and pore size is not confined to only shrink during densification. As a matter of fact, pores were repeatedly found to grow during the intermediate stage of sintering [39, 49, 50]. If pores only shrank but not grew with grain growth, grain growth itself would have led to densification. However, this is impossible.

(3) Some equation derivation errors as can be identified in Coble's paper [12, 13] were avoided in the present paper. For example, Equation 8 in Ref. [12] is:

$$P_c \cong r^2/l^2 \approx 10D\gamma a_0^3(t_f - t)/l^3 \qquad \text{(a)}$$

and the meanings of the symbols in the equation can be found in Ref. [12]. The equation was integrated with respect to time under the assumption of fixed l ($l =$ grain size, here l was a constant), however, the relation $l^3 =$ At (note: l here became a function of time) was later combined into the equation, and the following equation derived:

$$\mathrm{d}P/\mathrm{d}t = ND\gamma a_0^3/l^3kT = ND\gamma a_0^3/AkTt \qquad \text{(b)}$$

and Equation 3 in Ref. [13] was afterwards obtained:

$$P = P_0 - ND\gamma a_0^3[\ln t/t_0]/AkT \qquad \text{(c)}$$

It is apparent that the above derivation involved some basic errors. The linear relation between porosity and the logarithm of time will not be obtained if the assumption of fixed l or alternatively the relation $l^3 =$ At were used throughout the whole equation derivation process.

(4) The present densification equations qualitatively show that during heating with a certain rate a maximum densification rate can be obtained and after that the densification decreases and will decrease to nearly zero at nearly theoretical densities. This basic sintering phenomenon has been repeatedly observed in practice [51–53], however, Coble's equations are not consistent with these observations.

Though the linear relation between densities and the logarithm of time are observed both in pressureless sintering and hot-pressing, the explanation still lacks a physical basis. Coble's equation fitted the relation, but would have not if derived strictly. As a matter of fact, the phenomenological relation can hardly be related to densification kinetics because the slope of the linear relation is almost independent on the temperature, both for pressureless sintering [54] and hot-pressing

[22]. Besides, as discussed in Section 1, other empirical equations in addition to this linear relation between densities and the logarithm of time were also found to be applicable in fitting the experimental data [18, 19, 25, 26]. From these points of view, efforts to fit the phenomenological relation from the thermodynamic and/or kinetic basis are not meaningful.

6. Applications of the densification equations

6.1. Densification equations applied to hot-pressing

Densification models describing the hot-pressing process can be roughly divided into two categories: (a) material flow models: materials are regarded as fluids and densification proceeds via viscous or plastic flow under the applied stress [22, 55]; (b) material diffusion models: densification proceeds via diffusion enhanced by the external pressure [23, 56]. Diffusional models were proposed to be either grain boundary diffusion controlled (Coble creep model) or lattice diffusion controlled (Nabarro-Herring creep model) [57]. The use of the pressureless sintering equations by Coble [12, 13] for the sintering process in hot-pressing is not possible. Another disadvantages of the Coble proposed model is that, in final stage of sintering, as the pore radius decreases, and the densification rate will reciprocally increase, and the densification rate will become infinite at full densification. The spherical pore model presented here by the present author can be directly applied to the densification process for hot-pressing, simply by adding the effective stress, σ_{eff}, from the external applied pressure into Equation 22 and the following related equations. The relation between the effective stress, σ_{eff} and the external applied pressure, P_{a}, will be simply assumed to be:

$$\sigma_{\text{eff}} = P_{\text{a}}(1-\rho)/4 \tag{53}$$

for uniaxial hot pressing, here $1/4$ stands for the ratio between the maximum section area ($1/4\pi d^2$) to the surface area (πd^2) of a particle; and

$$\sigma_{\text{eff}} = P_{\text{a}}(1-\rho) \tag{54}$$

for isostatical hot pressing. So the total compressive stress on a pore will be:

$$\sigma_{\text{P}} = \frac{4\gamma_{\text{s}}P}{RD}\left[1-(R+1)\cos\frac{\phi_{\text{e}}}{2}+\frac{\sigma_{\text{eff}}RD}{4\gamma_{\text{s}}\rho}\right] \tag{55}$$

Combining Equations 35 and 55, the densification rate can be written as

$$\frac{\mathrm{d}\rho}{\rho\,\mathrm{d}t} = \frac{48K\rho^2(1-\rho)^{1/3}\Omega_{\text{a}}D_{\text{eff}}\gamma_{\text{s}}}{D^3\left[(K\rho)^{1/3}+(1-\rho)^{1/3}\right]kT} \times\left\{1-\left[(K\rho)^{-1/3}(1-\rho)^{1/3}+1\right] \times\cos\frac{\phi_{\text{e}}}{2}+\frac{\sigma_{\text{eff}}RD}{4\gamma_{\text{s}}\rho}\right\} \tag{56}$$

As the external pressure is usually much larger than the stress arising from surface tension or interface energy, so Equation 56 can be further simplified to be:

$$\frac{\mathrm{d}\rho}{\rho\,\mathrm{d}t} = \frac{12(K\rho)^{2/3}(1-\rho)^{2/3}\Omega_{\text{a}}D_{\text{eff}}}{D^2\left[(K\rho)^{1/3}+(1-\rho)^{1/3}\right]kT}\sigma_{\text{eff}} \tag{57}$$

So it can be seen that the new model is equivalent to the lattice diffusion model (Nabarro-Herring creep model) [57], and moreover, the equation can be directly used either for the intermediate stage of sintering or the final stage of sintering. The equation shows that as the relative density approaches 100%, the densification rate will be zero.

The densification equations (Equations 56 and 57) also show that, for the densification process in hot pressing, as the external pressure which exerts the compressive stress on pores is usually much larger than that by either surface or interface tension, the effect of pore size distribution and the dihedral angle are negligible. Therefore parameters such as surface and interface energy can be neglected and the phenomenological equations, e.g., material flow equations, are also applicable to the sintering process of hot-pressing [22].

6.2. Densification applied to liquid phase sintering

Liquid phase sintering has been investigated much longer than solid state sintering [58, 59]. Generally material flow mechanisms on macroscopical level were used for the description of the densification behaviour in liquid phase sintering. However, it is believed that the material diffusion mechanism on microstructural level could be also applied for liquid phase sintering. Under the conditions that the particle rearrangement arising from the capillary force were not considered, the model proposed in this paper for solid state sintering is tried for liquid phase sintering as follows.

6.2.1. Liquid can wet both particle interface and surface

To wet the interface and surface at the same time, the content of liquid phase should be high enough, and, the condition of $\gamma_{\text{l}}+\gamma_{\text{ls}}<\gamma_{\text{s}}$ and $2\gamma_{\text{ls}}<\gamma_{\text{ss}}$ should be satisfied simultaneously, here γ_{l}, γ_{ls}, γ_{s}, γ_{ss} are the surface tension of liquid, interface tension between solid and liquid phases, surface tension of solid and the interface tension between solid particles. Under the condition the liquid phase can form a continuous network in three dimension and cover all the surfaces and interfaces of solid particles. Therefore in this case the dihedral angle is 180°, the driving force for densification is the surface tension of liquid and no resistance is present for pore shrink, so Equation 38 can be modified as:

$$\frac{\mathrm{d}\rho}{\rho\,\mathrm{d}t} = \frac{48\rho(1-\rho)\Omega_{\text{a}}D_{\text{eff}}\gamma_{\text{l}}}{D^3\bar{R}^2(\bar{R}+1)kT}\left[1-(\bar{R}+1)\cos\frac{\phi_{\text{e}}}{2}\right] = \frac{48\rho(1-\rho)\Omega_{\text{a}}D_{\text{eff,l}}\gamma_{\text{l}}}{D^3\bar{R}^2(\bar{R}+1)kT} \tag{58}$$

here $D_{\text{eff,l}}$ is the diffusion coefficiency of species in liquid phase. In this case all pores can be removed thermodynamically.

6.2.2. Liquid can wet only particle interface

When there is appropriate amount of liquid phase and the condition of $\gamma_{\text{l}} + \gamma_{\text{ls}} > \gamma_{\text{s}}$ and $2\gamma_{\text{ls}} < \gamma_{\text{ss}}$ can be satisfied, liquid phase can only spread into the interface between particles, all solid interface were wetted with liquid while surface remain unwetted. In this case the driving force for densification is the surface tension of solid phase while the resistance is the interface tension between liquid and solid phases, there will be the following densification equation:

$$\frac{\mathrm{d}\rho}{\rho\,\mathrm{d}t} = \frac{48\rho(1-\rho)\Omega_{\text{a}} D_{\text{eff,l}}\gamma_{\text{s}}}{D^3\bar{R}^2(\bar{R}+1)kT}\left[1-(\bar{R}+1)\cos\frac{\phi_{\text{e,sl}}}{2}\right] \tag{59}$$

here $\phi_{\text{e,sl}}$ is the dihedral angle between solid surface and liquid interface. As in this case two liquid-solid interface tensions are balanced by solid surface tension, the dihedral angle will be expressed as:

$$\cos\frac{\phi_{e,sl}}{2} = \frac{\gamma_{\text{ls}}}{\gamma_{\text{s}}} \tag{60}$$

In the above two cases the surface and/or interface can be well wetted. Considering the much higher diffusion ability in liquid than in solids (this is approximately equivalent to the concept of "solution-precipitation" process [59] used in liquid phase sintering), the densification process will be accelerated as compared to solid state sintering through the process of mass transport via liquid phase, and the sintering temperature can therefore be lowered significantly.

6.2.3. Liquid phase can wet neither surface nor interface

In this case there is no capillary force of the liquid phase which can act as the driving force for particle rearrangement. The liquid phase cannot act as the diffusion path of solid species, in contrast it may act as the impedance for the diffusion of solid species. Therefore though there is rarely such cases, once such a situation is present, the densification is believed to be greatly retarded. For example, when about 1 wt % sodium oxide were added into Y-TZP powder, the densification of the materials were greatly affected [60].

7. Conclusion

1) The stability of a two-dimensional pore can be determined by a mathematical relation of the curvature of the pore-particle surface, coordination number, and dihedral angle. The stability of a space pore can be approximately determined by a spherical pore model, and has been found to be related to the dihedral angle, particle coordination number, and the size ratio of the pore to its surrounding particles.

2) Based on the spherical pore model, pore microstructure models for sintering were developed both for the intermediate and final stages of sintering.

3) Densification equations for the intermediate and final stages of solid state sintering are derived by relating densification to pore to particle size ratio, and used for the understanding of the densification process. The criterion for pore shrinkage was obtained.

4) The derived equations can be used for the explanation of the effect of pore size distribution, agglomeration properties, the density of the green compacts and entrapped gas in the final stage on sintering.

5) The derived densification equations can be easily developed for sintering process of hot-pressing or isostatic-hot-pressing. The results show that the densification equations for hot-pressing fit the lattice creep model.

6) Efforts were made to apply the densification equations for solid state sintering to liquid phase sintering under several different wetting conditions between liquid phase and solid particle phase.

References

1. C. HERRING, *J. Appl. Phys.* **21** (1950) 301.
2. G. C. KUCZYNSKI, N. A. HOOTEN and G. N. GILBSON (ed.), "Sintering and Related Phenomena" (Gorden & Breach, New York, 1967).
3. G. C. KUCZYNSKI (ed.), "Sintering and Related Phenomena," Mater. Sci. Res., Vol. 6 (Plenum, New York, 1973).
4. A. R. COOPER and A. H. HEUER (eds.), "Mass Transport Phenomena in Ceramics," Mater. Sci. Res., Vol. 9 (Plenum Press, New York and London, 1975).
5. G. C. KUCZYNSKI (ed.), "Sintering and Catalysis," Mater. Sci. Res., Vol. 10 (Plenum Press, New York and London, 1978).
6. *Idem.*, (ed.), "Sintering Process," Mater. Sci. Res., Vol. 13 (Plenum Press, New York and London, 1980).
7. J. PASK and A. EVANS (eds.), "Surfaces and Interfaces in Ceramic and Ceramic Metal Systems," Mater. Sci. Res., Vol. 14 (Plenum Press, New York and London, 1981).
8. D. KOLAR, S. PEJOVNIK and M. M. RISTIC (eds.), "Sintering—Theory and Practice," Mater. Sci. Monographs, Vol. 14 (Elsevier, Amsterdam, 1982).
9. M. M. RISTIC and B. KIDRIC (eds.), "Physics of Sintering," Vol. 5 (Institute of Nuclear Science, Beograd, Yugoslavia, 1973).
10. S. SOMIYA and SHIMADA (eds.), "Sintering 87" (Elsevier Applied Science, London, 1988).
11. S. SOMIYA and Y. MORIYOSHI (eds.), "Sintering, Key Papers" (Elsevier Applied Science, London, 1987).
12. R. L. COBLE, *J. Applied Physics* **32**(5) (1961) 787–793.
13. *Idem.*, *ibid.* **32**(5) (1961) 793.
14. G. C. KUCZYNSKI, AIME **85** (1949) 169–178.
15. *Idem.*, in "Sintering, Key Papers," edited by S. Somiya and Y. Moriyoshi (Elsevier Applied Science, London, 1987) pp. 501–508.
16. W. D. KINGERY and M. BERG, *J. Appl. Phys.* **26**(10) (1955) 1205–1212.
17. J. A. PASK, in "Sintering, Key Papers," edited by S. Somiya and Y. Moriyoshi (Elsevier Applied Science, London, 1987) pp. 567–678.
18. H. E. EXNER, *Powder Metallurgy* **4** (1980) 203–209.
19. H. E. EXNER and E. ARZT, in "Physical Metallurgy," edited by R. W. Cahn and P. Haasan, 3rd ed. (Elsevier Science Publishers BV, 1983) Chap. 10, pp. 1185–1912; in "Sintering, Key Papers," edited by S. Somiya and Y. Moriyoshi (Elsevier Applied Science, London, 1987) pp. 157–184.
20. W. S. COBLENZ, J. M. DYNYS, R. M. CANNON and R. L. COBLE, in "Sintering Process," Mater. Sci. Res., Vol. 13, edited by G. C. Kuczynski (Plenum Press, New York and London, 1980) pp. 141–157.
21. D. L. JOHNSON, *J. Amer. Ceram. Soc.* **53**(10) (1970) 574–577.
22. J. L. SHI and Z. X. LIN, *Ceram. Int.* **15** (1989) 107–112.
23. J. M. VIEIRA and R. J. BROOK, *J. Amer. Ceram. Soc.* **67**(2) (1984) 245–249.

24. *Idem.*, *ibid.* **67**(7) (1984) 450–454.
25. H. E. EXNER and G. PETZOW, in "Sintering Processes," Mater. Sci. Res., Vol. 13, edited by G. C. Kuczynski (Plenum, New York, 1980) pp. 107–120.
26. S. PEJOVNIK, V. SMOLEJ, D. SUSNIK and D. KOLAR, *Powder Metall. Int.* **11** (1979) 22–24.
27. M. H. TIKKANEN and S. A. MAKIPIRTTI, *Int. J. Powd. Met.* **1**(1) (1965) 15–22.
28. M. P. HARMER, H. M. CHAN and D. M. SMYTH, in "Defect Properties and Processing of High-Technology Nonmetallic Materials," edited by Y. Chen, W. D. Kingery and R. J. Stokes (Materials Research Society, Pittsburgh, Pennsylvania, 1986) pp. 125–134.
29. M. P. HARMER, in "Advances in Ceramics," Vol. 10 (American Ceramic Society, Columbus, OH, 1985) pp. 679–696.
30. F. V. LEVEL, in "Sintering, Key Papers," edited by S. Somiya and Y. Moriyoshi (Elsevier Applied Science, London, 1987), pp. 543–566.
31. G. C. KUCZYNSKI, in "Sintering—Theory and Practice," Mater. Sci. Monographs, Vol. 14 (Elsevier, Amsterdam, 1982) pp. 37–44.
32. T. T. FANG and H. PALMER III, *Ceram. Int.* **15** (1989) 329–335.
33. W. D. KINGERY and B. FRANCOIS, in "Sintering and Related Phenomena," edited by G. C. Kuczynski, N. A. Hooten and G. N. Gilbson (Gorden & Breach, New York, 1967) pp. 471–498.
34. F. F. LANGE, *J. Amer. Ceram. Soc.* **67** (1984) 83.
35. J. L. SHI, J. H. GAO, Z. X. LIN and T. S. YEN, *ibid.* **74**(5) (1991) 994–997.
36. F. F. LANGE and B. J. KELLET, *ibid.* **72**(5) (1989) 735–741.
37. B. J. KELLET and F. F. LANGE, in "Advanced Ceramic Processing and Technology," Vol. 1, edited by J. G. P. Binner (Noyes Publications, 1990) pp. 1–38.
38. T. K. GUPTA, *J. Amer. Cera. Soc.* **55**(5) (1972) 176–177.
39. J. L. SHI, "Solid State Sintering of Ceramics: Experimental Tests on Grain Growth, Pore Growth and Densification of Superfine Zirconia Powders," to be published.
40. C. HERRING, in "The Physics of Powder Metallurgy," edited by T. E. Kingston (McGraw-Hill, New York, 1951) chap. 8, p. 143.
41. R. L. EADIE and G. C. WEATHERLY, in "Sintering and Catalysis," edited by G. C. Kuczynski (Plenum Press, New York, 1978) pp. 239–248.
42. D. L. JOHNSON, in "Sintering Processes," Mater. Sci. Res., Vol. 13, edited by G. C. Kuczynski (Plenum, New York, 1980) pp. 97–104.
43. *Idem.*, in "Processing of Crystalline Ceramics," Materials Science Research, Vol. 11, edited by H. Palmour III, R. F. Davis and T. M. Hare (Plenum Press, New York, 1978) pp. 137–149.
44. J. ZHENG and J. S. REED, *J. Amer. Ceram. Soc.* **72**(5) (1989) 810–817.
45. J. L. SHI, Z. X. LIN and T. S. YEN, *J. Mater. Sci.* **28**(2) (1993) 342–348.
46. B. FRANCOIS and W. D. KINGERY, "Physical Metallurgy," edited by R. W. Cohn and P. Haasan, 3rd ed. (Elsevier Science Publishers BV, 1983) pp. 499–525.
47. J. ZHAO and M. P. HARMER, *J. Amer. Ceram. Soc.* **71**(7) (1988) 530–539.
48. A. G. EVANS, *ibid.* **65**(10) (1982) 498–506.
49. O. J. WHITTEMORE and J. A. VARELA, in "Sintering—Key Papers," edited by S. Somiya and Y. Moriyoshi (Elsevier Applied Science, London 1987) pp. 777–793.
50. J. A. VARELA, O. J. WHITTEMORE and E. LONGO, *Ceram. Int.* **16** (1990) 177–189.
51. F. F. LANGE, in "Ceramic Transactions Vol. 1, Ceramic Powder Science," edited by G. L. Messing, E. R. Fuller and H. Hausner (The American Ceramic Soc. Westerville, OH, 1987) pp. 1069–1083.
52. J. L. SHI and T. S. YEN, *J. Europ. Ceram. Soc.* **15**(4) (1995) 363–369.
53. J. L. SHI, Z. X. LIN and T. S. YEN, *J. Mater. Sci.* **28**(2) (1993) 342–348.
54. J. L. SHI and T. S. YEN, *J. Europ. Ceram. Soc.* **14** (1994) 505–510.
55. R. M. SPRIGGS, in "Sintering and Related Phenomena," Mater. Sci. Res., Vol. 6, edited by G. C. Kuczynski (Plenum, New York, 1973) pp. 369–379.
56. R. L. COBLE, *J. Appl. Phys.* **41**(12) (1970) 4798–4807.
57. F. R. N. NABARRO, *The Physical Soc.* (1948) 75–90.
58. W. D. KINGERY, *J. Appl. Phys.* **30**(3) (1959) 301–306.
59. G. PETZOW and W. A. KAYSSER, in "Sintered Metal-Ceramic Composites," edited by G. S. Upadhyaya (1984) pp. 51–70.
60. J. L. SHI, T. S. YEN and H. SCHUBERT, *J. Mater. Sci.* **32** (1997) 1341–1346.

Received 26 August 1997
and accepted 30 November 1998